LAWRENCE
LIVERMORE
NATIONAL
LABORATORY

LLNL-JRNL-482755

Computing and Partitioning Cloud Feedbacks using Cloud Property Histograms. Part II: Attribution to the Nature of Cloud Changes

M. D. Zelinka, S. A. Klein, D. L. Hartmann

May 4, 2011

Journal of Climate

Disclaimer

Computing and Partitioning Cloud Feedbacks using Cloud Property Histograms.

Part II: Attribution to the Nature of Cloud Changes

Mark D. Zelinka *

Department of Atmospheric Sciences, University of Washington, Seattle, Washington,

and Program for Climate Model Diagnosis and Intercomparison, Lawrence Livermore National Laboratory, Livermore, California

Stephen A. Klein

Program for Climate Model Diagnosis and Intercomparison, Lawrence Livermore National Laboratory, Livermore, California

Dennis L. Hartmann

Department of Atmospheric Sciences, University of Washington, Seattle, Washington

* *Corresponding author address:* Mark D. Zelinka, Program for Climate Model Diagnosis and Intercomparison Lawrence Livermore National Laboratory 7000 East Avenue, L-103 Livermore, CA 94551
E-mail: zelinka1@llnl.gov

ABSTRACT

Cloud radiative kernels and histograms of cloud fraction, both as functions of cloud top pressure and optical depth, are used to quantify cloud amount, cloud height and cloud optical depth feedbacks. The analysis is applied to doubled CO_2 slab-ocean simulations from ten global climate models participating in the Cloud Feedback Model Intercomparison Project. In the ensemble mean, total cloud amount decreases, especially between 55°S and 60°N, cloud altitude increases, and optical depths increase poleward of about 40° and decrease at lower latitudes. Both longwave (LW) and shortwave (SW) cloud feedbacks are positive, with the latter nearly twice as as large as the former. We show that increasing cloud top altitude is the dominant contributor to the positive LW cloud feedback, and that the extra-tropical contribution to the altitude feedback is approximately 70% as large as the tropical contribution. In the ensemble mean, the positive impact of rising clouds is 50% larger than the negative impact of reductions in cloud amount on LW cloud feedback, but the degree to which reductions in cloud fraction offset the effect of rising clouds varies considerably across models. In contrast, reductions in cloud fraction make a large and virtually unopposed positive contribution to SW cloud feedback, though the inter-model spread is greater than for any other individual feedback component. In general, models exhibiting greater reductions in subtropical marine boundary layer cloudiness tend to have larger positive SW cloud feedbacks, in agreement with previous studies. Overall reductions in cloud amount have twice as large an impact on SW fluxes as on LW fluxes such that the net cloud amount feedback is moderately positive, with no models analyzed here having a negative net cloud amount feedback. As a consequence of large but partially offsetting effects of cloud amount reductions on LW and SW feedbacks, increasing cloud altitude

actually makes a greater contribution to the net cloud feedback than does the reduction in cloud amount. Furthermore, the inter-model spread in net cloud altitude feedback is actually larger than that of net cloud amount feedback. Finally, we find that although global mean cloud optical depth feedbacks are generally smaller than the other components, they are the dominant process at high latitudes. This large negative optical depth feedback at high latitudes appears to result from a combination of increased cloud water content and changes in phase from ice to liquid, not from increases in total cloud amount associated with the poleward shift of the storm track, as is commonly assumed.

1. Introduction

Since the early days of climate modeling it has been recognized that changes in clouds that accompany climate change provide a feedback through their large impact on the radiation budget of the planet. As early as 1974, it was noted that accurate assessment of cloud feedback requires quantifying the spatially-varying role of changes in cloud amount, height, and optical properties on both shortwave (SW) and longwave (LW) radiation and that even subtle changes to any of these properties can have significant effects on the planetary energy budget (Schneider and Dickinson (1974)). Schneider (1972) performed one of the first investigations into the role of clouds as feedback mechanisms, focusing on hypothetical changes in cloud amount and height. His calculations showed that a negative feedback would be produced at most latitudes from an increase in low and middle-level clouds if albedo and height were held fixed but that this effect could largely be cancelled by the enhanced cloud greenhouse effect caused by a rise in global mean cloud top height of only a few tenths of

a kilometer, a result also supported by Cess (1974) and Cess (1975). Other early studies focused on the potential increase in cloud optical depth that would occur in association with global warming. Paltridge (1980), using the relationship between cloud optical depth and liquid water path derived by Stephens (1978), showed that increases in liquid water path would tend to strongly increase the amount of reflected SW radiation more than it would decrease the amount of emitted LW radiation, resulting in a strong negative feedback on a warming climate. These results were reinforced in the study of Somerville and Remer (1984), who derived a large negative optical depth feedback using a 1-D radiative-convective equilibrium model with empirically derived relations between temperature and cloud water content measured by aircraft over the former Soviet Union (Feigelson (1978)). The adiabatic increase of cloud liquid water path with temperature derived by Betts and Harshvardan (1987) lent theoretical support to a cloud optical depth feedback.

Although 1-D radiative-convective equilibrium models employed to quantify cloud feedback in early studies like those described above provide insight into potential cloud feedbacks, the cloud feedback operating in nature in response to external forcing is, as pointed out in Schneider et al. (1978), made up of a complex mix of time, space, and radiation-weighted cloud changes. The best chance to realistically simulate the response of clouds to external forcing is with fully three-dimensional global climate models (GCMs). Some of the pioneering investigations into cloud feedback processes occurring in full three-dimensional GCMs are those of Schneider et al. (1978) in the NCAR model, Manabe and Wetherald (1980) and Wetherald and Manabe (1980) in the GFDL model, and Hansen et al. (1984) in the GISS model. Inserting global mean cloud profiles produced by the GISS model for a control and doubled-CO_2 climate into the 1-D radiative convective equilibrium model of Lacis et al.

(1981), Hansen et al. (1984) calculated that cloud feedback represents a significant positive feedback, made up of roughly equal contributions from decreased outgoing longwave radiation due to increased cloud height and increased absorbed solar radiation due to decreased cloud amount. Similar patterns of cloud changes, namely, a reduction in low and middle level clouds and an increase in the height of tropical high clouds, were later found in the GFDL model by Wetherald and Manabe (1988). Using the partial radiative perturbation technique first introduced in Wetherald and Manabe (1980), they noted that the the LW cloud amount and height feedbacks tended to oppose one another, resulting in a positive LW cloud feedback that was roughly half as large as the positive SW cloud feedback.

Roeckner et al. (1987) performed the first doubled-CO_2 GCM experiments in which cloud liquid water was included prognostically, and found, after clarification by Schlesinger (1988), that increases in cloud liquid water path and optical depth brought about a positive LW optical depth feedback (due to increased high cloud emissivity) that dominated over the smaller negative SW optical depth feedback (due to increased cloud reflectivity). This result later received further support from the uniform ± 2 K sea surface temperature perturbation experiments of Taylor and Ghan (1992) for the NCAR model, but Senior and Mitchell (1993) found that phase changes from ice to water in doubled CO_2 experiments in the UK Met Office model brought about large negative SW cloud feedbacks (which they defined as the change in SW cloud radiative forcing), with contributions primarily coming from clouds at mid- and high-latitudes.

Colman et al. (2001), using an earlier version of the BMRC model, performed perhaps the most comprehensive analysis of cloud feedback due to a doubling of CO_2, separating the feedback into components due to changes in cloud amount, height, and optical depth,

with the latter further broken down into components due to changes in total water, phase, convective cloud fraction, and in-cloud temperature (a proxy for cloud geometric thickness). Using the partial radiative perturbation method of Wetherald and Manabe (1980), they computed large negative contributions to the LW cloud feedback from reductions in cloud fraction and positive contributions from changes in cloud height and optical depth, the latter dominated by increases in total water content of clouds. Conversely, they computed large positive contributions to the SW cloud feedback from reductions in cloud amount and increases in cloud height, but large negative contributions from increases in cloud optical depth, the latter being primarily due to phase changes from ice to liquid, with a smaller contribution from increases in total water content.

Though the issue of inter-model spread tends to dominate contemporary discussions of cloud feedback, it is also important to identify, quantify, and understand which aspects are robust and if there are fundamental physical explanations for such responses in a warming climate. Common features to nearly all GCM studies of global warming due to increasing greenhouse gas concentrations, including the early studies described above as well as the current generation of climate models (c.f., Figure 10.10 of Meehl (2007)), are a decrease in cloud amount equatorward of about 50°, an increase in cloud amount poleward of 50°, and an overall upward shift of clouds, features that mimic the average change in relative humidity. Zelinka and Hartmann (2010) have argued that estimates of LW cloud feedback in models taking part in CMIP3 are robustly positive and exhibit half as much inter-model spread as those of SW cloud feedback because of the tendency for tropical high clouds to rise in such a way as to remain at approximately the same temperature, a feature that Cess (1974) and Cess (1975) advocated as appropriate for accurately describing the sensitivity

of clouds to surface temperature, and that is well-explained by the constraints of radiative-convective equilibrium (Hartmann and Larson (2002)). Another feature that is emerging as fairly robust across models is the large increase in cloud optical depth in the region of mixed-phase clouds (roughly between 0° and -15°C) and smaller decrease at temperatures greater than freezing (Mitchell et al. (1989); Senior and Mitchell (1993); Tselioudis et al. (1998); Colman et al. (2001); Tsushima et al. (2006)).

In summary, models predict opposing effects on LW and SW radiation from changes in cloud amount, altitude, and optical depth. The net cloud feedback thus represents the integrated effect on radiation from spatially-varying – and in many cases subtle – cloud amount, altitude, and optical depth responses that individually may have large magnitudes and varying degrees of compensation. The relative magnitude of each of these processes depends greatly on the details of each model's cloud parameterization, such that even though most models produce a similar gross change in cloud distribution, estimates of cloud feedback remain widely spread relative to other feedbacks. Indeed, as first identified by Cess et al. (1989) and Cess (1990), the variation in climate sensitivities predicted by GCMs is primarily attributable to inter-model differences in cloud feedbacks. This continues to be the case in contemporary climate models (Colman (2003); Soden and Held (2006); Ringer et al. (2006); Webb et al. (2006)), and recent evidence has identified the response of marine boundary layer clouds in subsidence regimes of the subtropics as primarily responsible for the inter-model spread in cloud feedback (e.g., Bony et al. (2004); Bony and Dufresne (2005); Wyant et al. (2006); Webb et al. (2006)). As we have noted in Part I, however, this should not be taken as evidence that other cloud responses are consistently modelled or make a narrow range of contributions to the feedback. The change in cloud properties and corresponding

cloud feedbacks are also likely to be strongly dependent on biases in their properties in the unperturbed state, as pointed out by Trenberth and Fasullo (2010) for clouds in the high latitudes of the Southern Hemisphere. Attribution of the mean and spread in cloud feedbacks to the *nature* of the cloud changes from which they arise, which is the purpose of this paper, is a necessary first step in identifying their robust and non-robust aspects and ultimately in identifying which aspects are physically plausible and therefore realistic.

In Part I of this study (Zelinka et al. (2011a, manuscript submitted to *J. Climate*) we proposed a new technique for computing cloud feedback using cloud radiative kernels along with histograms of cloud fraction partitioned into CTP and τ bins by the International Satellite Cloud Climatology Project (ISCCP) simulator (Klein and Jakob (1999); Webb et al. (2001)). The technique has numerous appealing aspects, namely, the use of a standard radiative transfer model and definition of cloudiness across models, the ability to quantify the contribution to cloud feedback from individual cloud types, the exclusion of any clear-sky changes that would otherwise require complicated corrections to infer a pure cloud signal from changes in cloud radiative forcing, and the simplicity in the calculation that requires neither high temporal resolution model output nor complicated substitution techniques. Furthermore, cloud feedbacks computed with the cloud radiative kernels exhibit close agreement with estimates of cloud feedback computed using the adjusted change in cloud radiative forcing technique of Soden et al. (2008).

In this study, we extend further the capabilities of this technique to attribute cloud feedbacks to the nature of cloud changes from which they arise in an ensemble of ten GCMs taking part in the first phase of the Cloud Feedback Model Intercomparison Project (CFMIP1). Specifically, we use the cloud radiative kernels developed in Part I in combination with a

decomposition of the change in cloud fraction histograms to quantify the contribution from amount, height, and optical depth changes to the ensemble mean and inter-model spread in LW, SW, and net cloud feedbacks. Colman (2003), Soden and Held (2006), and Soden et al. (2008) have provided intercomparisons of global mean cloud feedbacks in the current generation of GCMs, but none have separately quantified the cloud amount, altitude, and optical depth feedbacks. Here we present the first model intercomparison of these components of cloud feedback.

2. Partitioning Cloud Feedback by Decomposing the Change in Cloud Distribution

We demonstrated in Part I that the cloud feedback estimated from the cloud radiative kernel technique compares well with the feedback estimated independently by adjusting changes in cloud radiative forcing for non-cloud effects using the technique outlined in Soden et al. (2008). We also made use of the highly detailed information provided in the histograms to partion the feedback into the various cloud types that cause it. However, the distinction between changes in cloud amount, height, and optical depth in contributing to cloud feedbacks remained ambiguous. For example, high cloud changes dominate the LW cloud feedback at all latitudes. This is unsurprising considering the high sensitivity of outgoing longwave radiation (OLR) to high clouds as shown by the cloud radiative kernel, so even if the total cloud fraction increased but the relative proportion of each cloud type in the histogram remained unchanged, high clouds would stand out as being of primary importance. It is more

interesting and illuminating to quantify the contribution to the positive LW cloud feedback of rising cloud tops relative to that of changes in total cloud amount holding the relative proportions fixed. Similarly, it is desirable to separate the role of proportionate changes in cloud fraction from that of a shift in the cloud optical depth distribution in contributing to both LW and SW cloud feedbacks. The decomposition of cloud fraction changes proposed here will remove some of the ambiguity associated with simply assessing cloud feedback from changes in cloud fraction in specific bins of the histogram.

In this section we present the methodology we use to decompose the change in cloud fraction into components due to the proportionate change in cloud fraction, the change in τ, and the change in CTP. The method is designed such that the feedback due to one of the three components (either cloud amount, altitude, or optical depth) is the result of only changes in that component with the other two components held fixed. To separate the effect of a change in mean cloud fraction from a shift in the altitude or optical depth of clouds, we divide the cloud fraction matrix into means over pressure and optical depth and departures therefrom. We note that several variants exist to define these feedbacks from ISCCP simulator output; we have chosen the most direct and simple method for our work, but we have seen little sensitivity to the method chosen. We will explain our methodology with the help of a 2x3 example matrix whose rows (columns) can be thought of as CTP (τ) bins. The technique described below is applied in an analogous way to the full 7x7 matrix of the ISCCP simulator output. In our example, the CTP-τ matrix of the joint histogram

of cloud fraction for a single location and month for the current climate is given by,

$$C = \begin{pmatrix} 2 & 3 & 1 \\ & & \\ 6 & 4 & 0 \end{pmatrix},$$

and an example matrix containing the change in cloud fraction, ΔC, between the current and 2xCO_2 climate for this location and month is given by

$$\Delta C = \begin{pmatrix} -1 & 0 & 2 \\ & & \\ 0 & 2 & 4 \end{pmatrix}.$$

The hypothetical change in cloud fraction assuming the change in total cloud fraction is distributed throughout the histogram such that the relative proportions of cloud fractions in each CTP-τ bin remains constant is computed as:

$$\Delta C_{prop} = (\frac{\Delta C_{tot}}{C_{tot}}) \times C. \tag{1}$$

ΔC_{tot} is the total change in cloud fraction computed as:

$$\Delta C_{tot} = \sum_{p=1}^{P} \sum_{\tau=1}^{T} \Delta C, \tag{2}$$

and C_{tot} is the total cloud fraction computed as:

$$C_{tot} = \sum_{p=1}^{P} \sum_{\tau=1}^{T} C, \tag{3}$$

where P and T are the number of CTP and τ bins in the histogram (in this example, 2 and 3, respectively). The first term in Equation 1 is a scalar representing the fractional change in total cloud fraction. This decomposition isolates the contribution of changes in total cloud fraction from changes in the vertical and optical depth distribution of clouds. Using the example values,

$$\Delta C_{prop} = \frac{7}{16} \times \begin{pmatrix} 2 & 3 & 1 \\ 6 & 4 & 0 \end{pmatrix} = \begin{pmatrix} 0.88 & 1.31 & 0.44 \\ 2.63 & 1.75 & 0.00 \end{pmatrix}.$$

The sum of the ΔC_{prop} histogram is exactly equal to the change in total cloud fraction, but constructed in such a way that the relative proportion of clouds in each bin remains constant. We will refer to ΔC_{prop} as the proportionate change in cloud fraction. To compute the cloud feedback associated it, which we refer to as the cloud amount feedback, we multiply this matrix by the corresponding entries of the cloud kernel for its location and month.

To compute the cloud altitude feedback, we compute the hypothetical change in the distribution of cloud fractions assuming the total cloud fraction as well as the relative proportion of cloud fraction in each τ bin remains constant. This is computed by performing the following subtraction at each pressure bin:

$$\Delta C_{\Delta p} = \Delta C - \frac{1}{P} \sum_{p=1}^{P} \Delta C \tag{4}$$

This computation takes the anomalous cloud fraction histogram and subtracts from each τ bin the mean anomaly across all CTP bins. This decomposition isolates the contribution of changes in the vertical distribution of clouds from the changes in total cloud fraction and

changes in the optical depth distribution of clouds. Using the example values,

$$\Delta C_{\Delta p} = \begin{pmatrix} -1 & 0 & 2 \\ 0 & 2 & 4 \end{pmatrix} - \begin{pmatrix} -0.50 & 1.00 & 3.00 \\ -0.50 & 1.00 & 3.00 \end{pmatrix} = \begin{pmatrix} -0.50 & -1.00 & -1.00 \\ 0.50 & 1.00 & 1.00 \end{pmatrix}$$

198 The sum of the $\Delta C_{\Delta p}$ histogram is exactly zero and the relative proportion of clouds in each
199 τ bin remains constant. Stated another way, C and $C + \Delta C_{\Delta p}$ have the same total amount
200 of cloud and relative proportion of clouds in each τ bin. Multiplying $\Delta C_{\Delta p}$ by the cloud
201 kernel for this location and month yields the cloud altitude feedback.

In a similar manner, to compute the optical depth feedback, we compute the hypothetical change in the distribution of cloud fractions assuming the total cloud fraction as well as the relative proportion of clouds in each CTP bin remains constant. This is computed by performing the following subtraction at each optical depth bin:

$$\Delta C_{\Delta \tau} = \Delta C - \frac{1}{T} \sum_{\tau=1}^{T} \Delta C \tag{5}$$

This computation takes the anomalous cloud fraction histogram and subtracts from each CTP bin the mean anomaly across all τ bins. This decomposition isolates the contribution of changes in the optical depth distribution of clouds from the changes in total cloud fraction and changes in the vertical distribution of clouds. Using the example values,

$$\Delta C_{\Delta \tau} = \begin{pmatrix} -1 & 0 & 2 \\ 0 & 2 & 4 \end{pmatrix} - \begin{pmatrix} 0.33 & 0.33 & 0.33 \\ 2.00 & 2.00 & 2.00 \end{pmatrix} = \begin{pmatrix} -1.33 & -0.33 & 1.67 \\ -2.00 & 0.00 & 2.00 \end{pmatrix}$$

202 The sum of the histogram is exactly zero and the relative proportion of clouds in each CTP

bin remains constant. Stated another way, C and $C + \Delta C_{\Delta\tau}$ have the same total amount of cloud and relative proportion of clouds in each CTP bin. Multiplying $\Delta C_{\Delta\tau}$ by the cloud kernel yields the cloud optical depth feedback.

The sum of the three decomposed matrices should roughly reproduce the true ΔC matrix. However, a small residual may remain in one or more bins (as in this example). Summing ΔC_{prop}, $\Delta C_{\Delta p}$, and $\Delta C_{\Delta\tau}$ gives

$$\begin{pmatrix} -0.96 & -0.02 & 1.10 \\ 1.13 & 2.75 & 3.00 \end{pmatrix}.$$

Note, however, that the sum of this matrix is constrained to exactly equal the true change in cloud fraction (7 in this example). The residual is

$$\Delta C_{residual} = \begin{pmatrix} -1 & 0 & 2 \\ 0 & 2 & 4 \end{pmatrix} - \begin{pmatrix} -0.96 & -0.02 & 1.10 \\ 1.13 & 2.75 & 3.00 \end{pmatrix} = \begin{pmatrix} -0.04 & 0.02 & 0.90 \\ -1.13 & -0.75 & 1.00 \end{pmatrix}.$$

Although the residual term sums to zero by design, it does contribute to the cloud feedback calculation because it is multiplied with the cloud radiative kernel before being summed. As shown below, this is generally a small contribution because the first-order components of the feedback are accounted for by the effect of cloud amount, altitude, and optical depth changes.

3. Ensemble Mean Change in Cloud Properties

As an aid in interpretting the contributions to cloud feedbacks from the three types of cloud changes decomposed above, in Figure 1 we show the ensemble mean change in total cloud fraction, CTP, and the natural logarithm of τ. The latter two quantities are computed by differencing the cloud fraction-weighted mean of the midpoints of each CTP or $\ln(\tau)$ bin between the control and doubled CO_2 climate. For simplicity, we will refer to these as changes in CTP and $\ln(\tau)$ rather than as changes in cloud fraction-weighted pressure and cloud fraction-weighted $\ln(\tau)$.

Cloud fraction decreases nearly everywhere between 55°S and 60°N and increases nearly everywhere poleward of these latitudes (Figure 1a). An exception to this pattern is a large region of increased cloud fraction in the central Equatorial Pacific which results from an eastward shift in convection tracking anomalously high SSTs. Cloud fraction reductions are prominent in the subtropics, especially over the continents. Large increases in cloud fraction tend to occur where regions formerly covered with sea ice become open water in the warmed climate. The general pattern of a decrease in cloud fraction equatorward of 50° is consistent with many previous studies (e.g., Wetherald and Manabe (1988); Senior and Mitchell (1993); Colman et al. (2001); Meehl (2007)).

Changes in CTP (Figure 1b) are negative nearly everywhere except in regions that become dominated by low cloud types (e.g., in the Arctic and in the Central Pacific just south of the Equator). Note that these values represent the change in cloud fraction-weighted pressure; thus a location in which the cloud regime changes between the two climates will exhibit large changes in this quantity (e.g., if the regime switches from being dominated by

low clouds to one dominated by high clouds). Therefore it is inappropriate to consider the value at every location on the map as representing a purely vertical shift with no influence from changing cloud types. However, that the global mean change in CTP is negative implies that clouds systematically rise as the planet warms. In the Tropics, this is consistent with theory (Hartmann and Larson (2002)) and results of cloud resolving model experiments (Kuang and Hartmann (2007); Tompkins and Craig (1999)) and other ensembles of GCM experiments (Zelinka and Hartmann (2010)). In the extratropics, rising clouds are also consistent with a rising tropopause from a warmer troposphere and colder stratosphere due to CO_2 (Kushner et al. (2001); Santer et al. (2003); Lorenz and DeWeaver (2007)).

The map of changes in $\ln(\tau)$ exhibits a remarkable structure characterized by large increases in $\ln(\tau)$ at latitudes poleward of about 40° and generally smaller decreases at low latitudes (Figure 1c). Increases in $\ln(\tau)$ associated with global warming extend farther equatorward over the continents and exhibit a large seasonal cycle (not shown) apparently driven by the larger seasonal variation in temperature relative to the oceans. As in the case of changes in CTP, it is important to keep in mind that the change in $\ln(\tau)$ does not distinguish between changes in cloud type and changes in optical thickness of a given cloud type. The optical depth changes produced in the models are qualitatively consistent with observationally-derived relationships between temperature and optical depth. Tselioudis et al. (1992) and Tselioudis and Rossow (1994) show using ISCCP data that cloud optical thickness increases with temperature for cold low clouds but decreases with temperature for warm low clouds. Additionally, Lin et al. (2003) show using data from the Surface Heat Budget of the Arctic Ocean (SHEBA) experiment that Arctic cloud *geometric* thickness tends to increase with surface temperature, resulting in clouds with larger optical thicknesses.

The high latitude cloud optical thickness response is likely related to changes in the phase and/or total water contents of clouds that lead to increases in optical thickness as temperature increases. As evidence, the fractional change in total, ice, and liquid water path is shown in Figure 2. The latter quantity is computed from the difference in the former two quantities. Due to limitations in the archive of CFMIP1 cloud output we cannot unambiguously separate these changes in grid-box mean water path into their contributions from changes in cloud amount or in-cloud water paths, much less directly relate these water path changes to optical depth changes. Nevertheless, large increases in total water path occur at high latitudes (Figure 2a), and are clearly dominated by the liquid phase (Figure 2c).

Several lines of evidence suggest that this is a realistic response of high latitude cloud properties, and that such changes should result in a clouds becoming more optically thick. The total water contents of liquid and ice clouds tend to increase with temperature in observations (Feigelson (1978); Somerville and Remer (1984); Mace et al. (2001)) at rates that may in some circumstances be related to the increase in adiabatic water content with temperature (Betts and Harshvardan (1987)). Betts and Harshvardan (1987) demonstrate analytically that the rate of change in cloud liquid water content as a function of temperature is twice as large at high latitudes compared with low latitudes. Additionally, a higher freezing level associated with a warmer atmosphere promotes more liquid phase clouds which – because of the Bergeron-Findeisen effect – tend to precipitate less efficiently and have larger water contents than ice or mixed-phase clouds (Senior and Mitchell (1993); Tsushima et al. (2006)). Finally, even if total water content were to remain constant, the smaller size of liquid droplets relative to ice crystals tends to enhance cloud reflectivity and therefore

increase optical depth.

4. Ensemble Mean Cloud Feedback Contributions

In Figure 3 we show the decomposed contributions to the ensemble and annual mean LW cloud feedback. In this and all of the following figures, the *uiuc* and *mpi_echam5* models are excluded for the reasons discussed in Part I, and the ensemble mean refers to the remaining ten models. Consistent with the results presented in Zelinka and Hartmann (2010), the change in the vertical distribution of clouds (i.e., rising cloud tops) is the dominant contributor to the LW cloud feedback (Figure 3c). A noteworthy feature is that the contribution of rising cloud tops to the LW cloud feedback is large not only within the Tropics but also in the extratropics. The extratropical (latitude $> 30°$) LW cloud altitude feedback is roughly 70% of that in the Tropics (0.37 and 0.52 W m^{-2} K^{-1}, respectively). Considering the robust increases in tropopause height in the extratropics with global warming (Kushner et al. (2001); Santer et al. (2003); Lorenz and DeWeaver (2007)) and the fact that most extratropical high cloud tops are near the tropopause, this may strengthen our confidence in the realism of rising extra-tropical clouds and their positive contribution to the LW cloud feedback. As in Zelinka and Hartmann (2010), we find that the ensemble mean contribution of rising tropical clouds to the LW cloud feedback (0.52 W m^{-2} K^{-1}) is twice as large as the global mean LW cloud feedback (0.26 W m^{-2} K^{-1}).

Globally, the impact of proportionate changes in cloud fraction on the LW cloud feedback is -0.30 W m^{-2} K^{-1} (Figure 3b), while the impact of increasing height of clouds is 0.45 W m^{-2} K^{-1}, 50% greater in magnitude. Though rising clouds remain the primary cause of LW

cloud feedback, reductions in total cloud amount offset more than half of the altitude effect. Positive LW cloud feedback that was primarily attributed to rising tropical cloud tops in Zelinka and Hartmann (2010) is supported here, but it is clear that rising extra-tropical clouds and reductions in cloud amount are also of primary importance in the global average. We are aware of no fundamental reasons to expect the upward shift to dominate over cloud fraction reductions in bringing about a positive LW cloud feedback, as observed here and in Zelinka and Hartmann (2010).

Finally, the contribution of changes in cloud optical depth is smaller in the global mean than that due to changes in cloud amount and height, but it is nonetheless positive nearly everywhere (Figure 3d). Notably, optical depth increases are the primary positive contribution to LW cloud feedback poleward of about 60° in both hemispheres, strongly opposing the locally negative altitude feedback over the polar oceans. In the global mean, the positive contribution to LW cloud feedback from optical depth increases is roughly equal to the combined contribution to LW cloud feedback from clouds rising and decreasing in fractional coverage.

In Figure 4 we show the decomposed contributions to the ensemble and annual mean SW cloud feedback. The dominant contributor to the SW cloud feedback at most locations and in the global mean is the change in cloud fraction holding the vertical and optical depth distribution fixed (Figure 4b). With the exception of the equatorial Pacific, where increases in cloud fraction occur in the ensemble mean, reductions in cloud fraction in most locations between 50°S and 65°N contribute to a positive SW cloud feedback. This is consistent with the results of Trenberth and Fasullo (2009), who showed reductions in low cloud fraction (as defined by the standard cloud fraction diagnostic provided by the modeling centers)

throughout this region coincident with increases in absorbed solar radiation over the 21^{st} Century.

Unsurprisingly, the impact of changes in cloud vertical distribution on SW fluxes is negligible everywhere (Figure 4c), though the global average value is slightly negative owing to the slight increase in SW flux sensitivity to cloud fraction changes with decreasing cloud top pressure (c.f., Figure 1b of Part I).

In the global mean, the SW optical depth feedback is considerably smaller than the SW cloud amount feedback, but is regionally very important (Figure 4d). In the tropical western Pacific, high clouds become thicker, thus causing a locally negative SW optical depth feedback. Elsewhere equatorward of about 40°, this feedback component is positive due to decreases in τ of low- and mid-level clouds. Consistent with this, Tselioudis et al. (1992), Tselioudis and Rossow (1994), and Chang and Coakley (2007) have shown using satellite observations that low- and midlatitude boundary layer clouds experience a decrease in optical depth as temperature increases. The most dramatic and robust feature of the optical depth feedback is the presence of large negative values at high latitudes in either hemisphere, which dominate the other contributions to SW cloud feedback. As discussed in the previous section, several lines of evidence suggest that cold clouds are particularly susceptible to increases in temperature that act to increase their optical depth, providing a possible physical basis for the modeled increases in τ (Figure 1c) and for the subsequent strong negative optical depth feedback at high latitudes shown here.

Trenberth and Fasullo (2010) assert that biases in the mean state of GCMs are leading to cloud feedbacks over the high southern latitudes that cannot be realized. Specifically, they argue that unrealistically small cloud fractions over the Southern Ocean in the mean state

permit unrealistically large cloud fraction increases as the planet warms. Here, however, we show that it is not the increase in cloud fraction but rather the shift towards brighter clouds that primarily causes this large negative cloud feedback. If cloud optical depth rather than cloud amount is biased low, then it is quite possible that models produce unrealistic increases in cloud brightness as the planet warms. Conversely, if cloud optical depth is biased high, as has been shown in many studies (e.g., Lin and Zhang (2004); Zhang (2005)) then the negative SW optical depth feedback is in fact *underestimated* compared to a model with more realistic mean state optical depths, as discussed in Bony et al. (2006). Regardless, as discussed above, several plausible explanations exist for why clouds, especially those at high latitudes, should become more optically thick as the planet warms. Thus we consider the simulated increases in reflected SW radiation found in the 50°-60°S latitude band to be plausible.

In Figure 5 we show the decomposed contributions to the ensemble and annual mean net cloud feedback, which is quite strongly positive (0.71 W m^{-2} K^{-1}). Surprisingly, the 0.41 W m^{-2} K^{-1} contribution of rising cloud tops (Figure 5c) exceeds the 0.36 W m^{-2} K^{-1} contribution of proportionate changes in the amount of clouds (Figure 5b) to net cloud feedback. This is not a trivial result. One could argue that fundamental constraints exist on cloud height and its changes, namely, the location of radiatively-driven clear-sky convergence in the tropics (Hartmann and Larson (2002); Zelinka and Hartmann (2010)), and the height of the tropopause in the extra-tropics (Kushner et al. (2001); Santer et al. (2003); Lorenz and DeWeaver (2007)), making this contribution to cloud feedback robust and relatively well-explained. The contribution of optical depth changes, though small in the global mean (0.09 W m^{-2} K^{-1}), is the primary cause of the large negative values of net cloud feedback

over the Arctic and Southern Ocean (Figure 5d). The effect of proportionate changes in cloud fraction as well as the effect of changes in the optical depth distribution of clouds on the net cloud feedback is dominated by the SW contribution (i.e., the net map looks like the SW map) whereas the effect of changes in the vertical distribution of clouds on the net cloud feedback is entirely due to the LW contribution (i.e., the net map looks like the LW map). Large positive contributions from both the reduction in total cloud fraction and the upward shift of clouds produces the positive net cloud feedback between 50°S and 65°N. The large negative contribution from the increase in cloud optical thickness produces the large negative cloud feedback over the Arctic and Southern Ocean.

That the cloud optical depth feedback dominates over the cloud amount feedback at high latitudes is a surprising result considering the large locally negative cloud feedback is often attributed (e.g., Weaver (2003); Vavrus et al. (2009); Wu et al. (2010)) to cloud fraction increases associated with the poleward-shifted storm track (Hall et al. (1994), Yin (2005)). Indeed, appreciable cloud fraction changes do occur at high latitudes (Figure 1a), and these do contribute to the negative SW cloud feedback, but this decomposition shows that the signal is dominated by increases in cloud optical thickness in this region, likely caused by the combination of large increases in total cloud water and phase changes (Figure 2). One must keep in mind, however, that the optical depth feedback as we have defined it does not distinguish a change in optical depth due to morphological changes in cloud type (e.g., from thin boundary layer clouds to thicker frontal clouds) that may be associated with a storm track shift from a change in optical depth due to a change in optical properties of the cloud types that are already present (e.g., thin boundary layer clouds becoming thicker).

To more completely illuminate the cloud changes that result in a change in cloud feedback

from positive to negative as one moves poleward, we show the changes that occur in the Southern Hemisphere where land does not obscure a clear zonal mean signal. In particular, we show the mean cloud fraction histograms in the control and doubled CO_2 climates, their difference, and the induced feedbacks for the 30°-50°S region in Figure 6 and for the 50°-70°S region in Figure 7. In both regions, the mean cloud fraction histogram primarily exhibits features of the stratocumulus, frontal, and cirrus regimes identified by Williams and Webb (2009), though clouds in the 50°-70°S region tend to be thinner and lower than those in the 30°-50°S region. The total cloud fraction is roughly 20% larger at 50°-70°S. The change in cloud fraction histogram that occurs due to climate change is remarkably different between these two regions (Figures 6c and 7c). At 30°-50°S, the primary change is a reduction in cloudiness at low levels and an increase in the altitude of high clouds. In contrast, at 50°-70°S, the primary change is an increase in cloudiness at large optical depths at all heights and decreases in the amount of low optical depth clouds, with an overall small increase in total cloudiness. An exception to this general shift of the distribution towards thicker clouds is in the lowest CTP bin (i.e., the highest clouds), where cloud fraction increases occur in every τ bin but more so at smaller optical depths, perhaps a signature of the increasing altitiude of high thin cirrus.

In the 30°-50°S region, increased cloudiness at the highest levels contributes to a small LW cloud feedback, but the positive contribution to SW cloud feedback from the large reductions in cloud amount in most bins dominates the cloud feedback. The impacts of high cloud changes on LW and SW fluxes largely offset each other, with the resultant large positive net cloud feedback being primarily caused by reduced SW reflection from the reduction in cloud at low and mid-levels. In contrast, at 50°-70°S, the shift towards thicker clouds gives

rise to a strong positive LW cloud feedback and negative SW cloud feedback, the latter having nearly the same magnitude as the positive SW cloud feedback at 30°-50°S. The effect of thickening high clouds on LW and SW fluxes largely offset each other and the net cloud feedback is dominated by the large shift towards thicker clouds at the lowest levels (likely stratocumulus clouds), making it moderately negative.

A striking feature that is apparent from comparing panels a and b of Figures 6 and 7 is the subtle nature of the changes that occur to the cloud fraction histograms in going from a control to a perturbed climate. Without computing a difference histogram (panel c) it is difficult to visually discern a difference in the mean cloud fraction histograms between the two climate states. The change in cloud distribution between the perturbed and control climate, though sufficiently large to induce significant effects on radiation, does not suggest a dramatic change in the types of clouds present in these regions. That such subtle changes in cloud distribution can produce large radiative fluxes is rather humbling in that it underscores an acute challenge of constraining cloud feedbacks.

The changes in cloud distribution that occur likely reflect some combination of changes in the relative proportion of cloud types present in each region and changes in the properties of the cloud types already present. Indeed, the results of Williams and Webb (2009) suggest that a combination of both processes is important in a similar ensemble of CFMIP1 models. Specifically, they find that the relative frequency of occurrence of thicker cloud types increases at the expense of thinner cloud types in high latitude regions, and that all high latitude cloud regimes except the thin cirrus regime experience a negative change in net cloud forcing.

The ensemble mean zonal mean cloud feedbacks and their partitioning among the three components described above (and the residual term not discussed above) are shown in Figure

8. The competing effects of rising cloud tops and decreasing cloud coverage on the LW cloud feedback is apparent at most latitudes, with the LW cloud altitude feedback dominating at most latitudes, especially in the deep Tropics and midlatitudes. Proportionate cloud changes are the dominant contributor to the SW cloud feedback at nearly every latitude, except at high latitudes where the large increase in optical depth dominates. The relative dominance of each contributor to the net cloud feedback varies as a function of latitude, but all components are generally positive except at high latitudes where the optical depth feedback is strong and negative.

In agreement with the physical mechanisms discussed above, Figure 7b of Colman et al. (2001) shows that the dominant contribution to the negative SW optical depth feedback at high latitudes in the BMRC model comes from cloud phase changes. They also note that the SW and LW cloud amount feedbacks oppose each other at most latitudes, with the global mean SW cloud amount feedback having a magnitude 2.2 times as large as that of the LW cloud amount feedback (-0.14 and 0.31 W m^{-2} K^{-1} for LW and SW, respectively). Remarkably, this is exactly the same ratio observed here for the ensemble mean cloud amount feedbacks (-0.3 and 0.66 W m^{-2} K^{-1} for LW and SW, respectively), and is also close to the ratio reported in Taylor and Ghan (1992).

5. Inter-Model Spread in Cloud Feedback Contributions

In Figure 9 we show bar plots of the global mean contributions of each component to the LW, SW, and net cloud feedbacks in each model. LW cloud feedback estimates span a range of 0.88 W m^{-2} K^{-1} (from -0.12 to 0.76 W m^{-2} K^{-1}), though only the *bmrc1* model has

a negative value. (Note that neither of the two tests for proper simulator implementation discussed in Part I could be performed for the *bmrc1* model.) In every model, proportionate reductions in global mean cloud fraction act to reduce the LW cloud feedback, with values spanning a range of 0.59 W m^{-2} K^{-1} (from -0.65 to -0.06 W m^{-2} K^{-1}). Increases in cloud top altitude contribute positively to the LW cloud feedback in all models, with values spanning a range of 0.74 W m^{-2} K^{-1} (from 0.06 to 0.80 W m^{-2} K^{-1}), a spread that warrants increased attention. Increases in cloud optical depth contribute positively to the LW cloud feedback in all models, with values spanning a range of 0.50 W m^{-2} K^{-1} (from 0.03 to 0.53 W m^{-2} K^{-1}).

Even though LW feedback is positive in all but one model, it is clear that the relative contribution of cloud fraction changes (negative feedback) and cloud vertical distribution changes (positive feedback) varies significantly between models. The ratio of the magnitude of the LW altitude feedback to the magnitude of the LW cloud amount feedback in individual models varies between 0.2 and 10.5. The high end is populated by models like *cccma_agcm4_0* and *ncar_ccsm3_0* that have very little cloud amount decrease and a large cloud-top pressure response whereas models like *bmrc1* and *ipsl_cm4* have the opposite proportionality. Thus, while the LW feedback may almost always be positive in models, the spread in this feedback and the relative role of cloud top pressure and cloud fraction responses does vary in a non-trivial way. Colman and McAvaney (1997) also found a widely varying amount of compensation between these two quantities, with resultant LW cloud feedbacks of different signs and magnitudes across four modified versions of the BMRC model. This demonstrates that large uncertainties remain in the response of clouds relevant to the LW cloud feedback, which, along with the result from Part I that the spread in high cloud-induced LW and SW

cloud feedback estimates exhibits more spread than that due to low clouds, suggests that the community should not focus solely on the implications of disparate responses of low cloud for cloud feedback.

SW cloud feedback estimates span a range of 1.16 W m^{-2} K^{-1} (from -0.13 to 1.03 W m^{-2} K^{-1}), though only the *gfdl_mlm2_1* model has a negative value. In all models, reductions in global mean cloud fraction act to increase the SW cloud feedback, with values spanning a range of 1.32 W m^{-2} K^{-1} (from 0.14 to 1.18 W m^{-2} K^{-1}). The range of estimates of this feedback component is the largest of all components among both the SW and LW cloud feedbacks. Increases in cloud top altitude contribute negatively to the SW cloud feedback in all models, but the values are very small, in no models exceeding -0.08 W m^{-2} K^{-1}. SW optical depth feedback estimates span a range of 0.80 W m^{-2} K^{-1} (from -0.58 to 0.22 W m^{-2} K^{-1}).

Net cloud feedback estimates are positive in all models, spanning a range of 0.92 W m^{-2} K^{-1} (from 0.22 to 1.14 W m^{-2} K^{-1}). Proportionate reductions in global mean cloud fraction act to give a positive net cloud feedback, with values spanning a range of 0.63 W m^{-2} K^{-1} (from 0.07 to 0.70 W m^{-2} K^{-1}). In every model, increases in cloud top altitude contribute positively to the net cloud feedback, with values spanning a range of 0.66 W m^{-2} K^{-1} (from 0.06 to 0.72 W m^{-2} K^{-1}). The strength of this component of the feedback has a larger inter-model spread than that of the cloud amount component, which is surprising considering the large focus placed on the implications of the disparate responses of subtropical boundary layer cloud amounts. Net optical depth feedback estimates span a range of 0.44 W m^{-2} K^{-1} (from -0.10 to 0.34 W m^{-2} K^{-1}). Only two models (*bmrc1* and *gfdl_mlm2_1*) have negative net optical depth feedbacks.

To display these results in a more compact manner, in Figure 10 we show global mean cloud feedback estimates and their partitioning among cloud amount, altitude, optical depth and residual components. As mentioned previously, the dominant contributor to the positive LW cloud feedback is the upward shift of clouds, with a smaller positive contribution from cloud thickening and a moderate negative contribution from cloud fraction decreases. Decreasing cloud amount makes by far the largest contribution to SW cloud feedback. Note that while the SW optical depth feedback makes little contribution to the global mean SW cloud feedback, it is the dominant feedback at high latitudes. Both the cloud altitude feedback and the cloud amount feedback contribute to the strong positive net cloud feedback. In the global mean, optical depth changes make a smaller positive contribution that is opposed by the negative effect of residual cloud changes.

Considerable inter-model spread is evident in most contributions to cloud feedback, with the SW cloud amount feedback exhibiting the largest spread. Due to the small sample size of only 10 models, regression coefficients of global mean cloud feedback components on global mean cloud feedback are indistinguishable from zero in most cases (regression slope uncertainty taken to be the 2σ range of the distribution of regression slopes computed using a bootstrapping method in which the predictand is resampled 1000 times). This demonstrates that inter-model spread is liberally distributed between component changes and LW and SW bands with no single component playing a dominant role. Two exceptions are the large positive regression coefficient between global mean SW cloud feedback and its amount component (0.77 ± 0.47) and large positive regression coefficient between global mean LW cloud feedback and its altitude component (0.62 ± 0.37). This leads to the result that models having greater positive SW cloud amount feedbacks (i.e., those with larger reductions in cloud

fraction) tend to have greater global mean SW cloud feedbacks and models having greater positive LW cloud altitude feedbacks tend to have greater positive LW cloud feedbacks. The spread in the LW cloud altitude feedback may be related to the inter-model spread in the vertical shift of peak radiatively-driven divergence in the Tropics and the tropopause height in the extratropics, which suggests that the spread in this feedback process can be explained simply by the spread in responses of models' vertical temperature structures. We do not attempt to demonstrate this here, as few models archived atmospheric temperature profiles; thus it remains speculation.

A regression of the global mean feedbacks on their values from each grid point can also be performed, highlighting the local contribution of each process to the spread in global mean cloud feedbacks, but at most locations, the regression slopes are statistically indistinguishable from zero. Regions that tend to be dominated by stratiform clouds over the subtropical oceans off the west coast of continents are among the regions (though not the only regions) for which the regression slope is significantly positive, indicating that an appreciable portion of the spread in global mean SW cloud feedback is attributable to the inter-model spread in the response of these clouds types. Models in which the SW cloud amount feedback is positive in these regions (i.e., models in which the amount of these clouds decreases) tend to be models having larger positive global mean SW cloud feedbacks, a result consistent with several others (Bony et al. (2004); Bony and Dufresne (2005); Wyant et al. (2006); Webb et al. (2006)).

6. Conclusions

We have proposed a decomposition of the change in cloud fraction histogram which separates cloud changes into components due to the proportionate change in cloud fraction holding the vertical and optical depth distribution fixed, the change in vertical distribution holding the optical depth distribution and total cloud amount fixed, and the change in optical depth distribution holding the vertical distribution and total cloud amount fixed. By multiplying the cloud radiative kernels developed in Part I with these decomposed changes in cloud fraction (normalized by the change in global mean surface temperature), we have computed the cloud amount, altitude, and optical depth feedbacks for an ensemble of ten models taking part in CFMIP1, allowing us to assess for the first time the relative roles of these processes in determining both the multi-model mean and inter-model spread in LW, SW, and net cloud feedback.

In agreement with many previous studies, a warmed climate is associated with a reduction in total cloud amount between about 55°S and 60°N, an increase in cloud amount poleward of these latitudes, an upward shift of clouds at nearly every location, an increase in cloud optical depth poleward of about 40°, and a generally much smaller decrease in cloud optical depth equatorward of 40°. We note that both changes in total water path and in phase from ice to liquid contributes to a shift towards brighter clouds at high latitudes, a feature that is in agreement with many studies (e.g., Somerville and Remer (1984); Betts and Harshvardan (1987); Tsushima et al. (2006)). However, we have noted that – even in regions where cloud changes are substantial enough to make large contributions to cloud feedback – a visual comparison of cloud fraction histograms in the control and perturbed climate reveals

a nearly indiscernible change in cloud properties. This highlights the concept that large changes in radiation can arise from very subtle cloud changes. A related point not explored here is that multi-decadal averages are necessary to discern these changes, which, while small, are still very important for cloud feedback.

Before summarizing our cloud feedback results, we wish to stress that our results are applicable specifically to this ensemble of ten global climate models coupled to slab oceans in which CO_2 is instantaneously doubled and the climate is allowed to re-equilibrate. Thus one should not expect perfect overlap between the estimates of cloud feedback shown here and those presented, for example, in Soden et al. (2008), who analyzed transient climate feedbacks computed as a difference between years 2000-2010 and 2090-2100 in an ensemble of 14 fully coupled ocean-atmosphere GCMs simulating the SRES A1B scenario, in which the concentrations of numerous radiative agents vary over the course of the century (Ramaswamy et al. (2001)), as well as among models (e.g., Collins (2006); Shindell et al. (2008)). Indeed, here we found a moderately large positive ensemble mean SW cloud feedback of 0.46 W m^{-2} K^{-1} and a LW cloud feedback that is roughly half as large, 0.26 W m^{-2} K^{-1}, whereas these values in GCMs simulating the SRES A2 scenario are 0.09 and 0.49 W m^{-2} K^{-1}, respectively (c.f., Figure 2 of Zelinka and Hartmann 2011a, manuscript submitted to *J. Climate*). While the exact values of global mean feedbacks may differ somewhat between the type of model run, we still expect that the important processes identified in this study to be relevant for other types of simulations such as transient climate change integrations of coupled ocean-atmosphere GCMs driven by gradual increases in greenhouse gases.

Rising clouds contribute positively to the LW cloud feedback in every model, and represent the dominant contributor to the positive ensemble mean LW cloud feedback, lending

further support to the conclusions of Zelinka and Hartmann (2010). Although that study focused solely on the contribution of rising tropical clouds to the positive LW cloud feedback, here we see that rising extratropical clouds also contribute significantly, with a contribution that is roughly 70% as large as that from tropical clouds. As a deeper troposphere is a consistently-modeled and theoretically-expected feature of a warming climate due to increased CO_2, the rise of clouds and its attendant large positive contribution to LW cloud feedback may be considered robust and well-explained. The impact of reductions in cloud amount on LW cloud feedback, however, systematically opposes that of increases in cloud altitude, and the ratio of the two components varies considerably between models, indicating that substantial inter-model variability exists in the response of high clouds, with implications for the size of LW cloud feedback. Nevertheless, in the ensemble mean, the LW cloud altitude feedback is roughly 50% larger than the LW cloud amount feedback. Interestingly, optical depth increases make a small positive contribution to the LW cloud feedback in every model, which, in the ensemble mean, is equal to the combined LW altitude plus amount feedback.

Overall reductions in cloud amount are by far the dominant contributor to the positive SW cloud feedback, and represent the largest individual contribution to the positive global mean cloud feedback in this ensemble of models. Although this component is positive in every model due to the robust reduction in global mean cloudiness, it exhibits the largest inter-model spread of all feedback components. The positive contribution from cloud amount reductions to SW cloud feedback is a little more than twice as large as the magnitude of its negative contribution to LW cloud feedback, highlighting the importance of reductions in low and middle level clouds. This factor of two is in remarkable agreement with results from both

the NCAR model experiment of Taylor and Ghan (1992) and the BMRC model experiment of Colman et al. (2001). Models with larger reductions in cloud amount in regions typically occupied by marine stratocumulus tend to have larger positive SW cloud feedbacks, a result in agreement with many previous studies (e.g., Bony et al. (2004); Bony and Dufresne (2005); Webb et al. (2006); Wyant et al. (2006)). The SW optical depth feedback is small globally, but is the dominant feedback at high latitudes, where the combination of increased cloud water content and phase change from ice to liquid increases the mean cloud optical depth. That the SW optical depth feedback dominates over the SW cloud amount feedback at high latitudes suggests that increases in net moisture transport and the liquid water content of clouds are more important than the poleward shift of the extratropical storm tracks that occurs in warming simulations.

The net cloud feedback represents the integrated effect of large, spatially heterogeneous, and in many cases opposing effects on the radiation budget. Nevertheless, it is positive in every model, as are the contributions from decreasing cloud amount and increasing cloud altitude. Interestingly, increasing cloud altitude makes a larger contribution to net cloud feedback than does decreasing cloud amount, and does so in seven out of ten models. This is because LW and SW cloud amount feedbacks tend to offset each other, while the positive impact of cloud height changes on the LW cloud feedback is largely unopposed. Although only two models have negative global mean optical depth feedbacks, all models exhibit large negative optical depth feedbacks at high latitudes. This locally large negative feedback is due primarily to low clouds becoming thicker, since the increased optical depth of high clouds has compensating effects on LW and SW radiation.

Acknowledgments.

This research was supported by the Regional and Global Climate Program of the Office of Science at the U. S. Department of Energy and by NASA Grant NNX09AH73G at the University of Washington. We acknowledge the international modeling groups, the Program for Climate Model Diagnosis and Intercomparison (PCMDI), and the WCRP's Working Group on Coupled Modelling (WGCM) for their roles in making available the WCRP CFMIP multi-model dataset. Support of this dataset is provided by the Office of Science, U.S. Department of Energy. We thank Brian Soden for providing the radiative kernels, Rick Hemler for providing additional *gfdl_mlm2_1* model output, Rob Wood, Chris Bretherton, and Robert Pincus for useful discussion and suggestions for improvement, and Marc Michelsen for computer support. This work was performed under the auspices of the U.S. Department of Energy by Lawrence Livermore National Laboratory under Contract DE-AC52-07NA27344.

REFERENCES

Betts, A. K. and Harshvardan, 1987: Thermodynamic constraint on the cloud liquid water feedback in climate models. *J. Geophys. Res.*, **92**, 8483–8485.

Bony, S. and J. L. Dufresne, 2005: Marine boundary layer clouds at the heart of tropical cloud feedback uncertainties in climate models. *Geophys. Res. Lett.*, **32**, L20806, doi: 10.1029/2005GL023851.

Bony, S., J. L. Dufresne, H. L. Treut, J. J. Morcrette, and C. Senior, 2004: On dynamic and thermodynamic components of cloud changes. *Climate Dyn.*, **22**, 71–68.

Bony, S., et al., 2006: How well do we understand and evaluate climate change feedback processes? *J. Climate*, **19**, 3445–3482.

Cess, R. D., 1974: Radiative transfer due to atmospheric water vapor: Global considerations of Earth's energy balance. *Journal of Quantitative Spectroscopy and Radiative Transfer*, **14 (9)**, 861–871.

Cess, R. D., 1975: Global climate change - investigation of atmospheric feedback mechanisms. *Tellus*, **27 (3)**, 193–198.

Cess, R. D., et al., 1989: Interpretation of cloud-climate feedback as produced by 14 atmospheric general circulation models. *Science*, **245 (4917)**, 513–516.

669 Cess, R. D. e. a., 1990: Intercomparison and interpretation of cloud-climate feedback pro-
670 cesses in nineteen atmospheric general circulation models. *J. Geophys. Res.*, **95**, 16 601–
671 16 615.

672 Chang, F.-L. and J. A. Coakley, 2007: Relationships between marine stratus cloud optical
673 depth and temperature: Inferences from AVHRR observations. *J. Climate*, **20 (10)**, 2022–
674 2036.

675 Collins, W. D. e. a., 2006: Radiative forcing by well-mixed greenhouse gases: Estimates
676 from climate models in the Intergovernmental Panel on Climate Change (IPCC) Fourth
677 Assessment Report (AR4). *J. Geophys. Res.*, **111**, D14317, doi:10.1029/2005JD006713.

678 Colman, R., 2003: A comparison of climate feedbacks in general circulation models. *Climate*
679 *Dyn.*, **20**, 865–873.

680 Colman, R., J. Fraser, and L. Rotstayn, 2001: Climate feedbacks in a general circulation
681 model incorporating prognostic clouds. *Climate Dyn.*, **18**, 103–122.

682 Colman, R. and B. McAvaney, 1997: A study of general circulation model climate feedbacks
683 determined from perturbed sea surface temperature experiments. *J. Geophys. Res.*, **102**,
684 19 383–19 402.

685 Feigelson, E. M., 1978: Preliminary radiation model of a cloudy atmosphere. Part I: Structure
686 of clouds and solar radiation. *Beitr. Phys. Atmos.*, **51**, 203–229.

687 Hall, N. M. J., B. J. Hoskins, P. J. Valdes, and C. A. Senior, 1994: Storm tracks in a high-
688 resolution gcm with doubled carbon dioxide. *Quart J Roy Meteorol Soc*, **120**, 1209–1230.

689 Hansen, J., A. Lacis, D. Rind, G. Russell, P. Stone, I. Fung, R. Ruedy, and J. Lerner, 1984:
690 Climate processes and climate sensitivity: Analysis of feedback mechanisms. *Geophys.*
691 *Monogr.*, **29**, 130–163.

692 Hartmann, D. L. and K. Larson, 2002: An important constraint on tropical cloud-climate
693 feedback. *Geophys. Res. Lett.*, **29 (20)**, doi:10.1029/2002GL015835.

694 Klein, S. A. and C. Jakob, 1999: Validation and sensitivities of frontal clouds simulated by
695 the ECMWF model. *Mon. Weath. Rev.*, **127**, 2514–2531.

696 Kuang, Z. and D. L. Hartmann, 2007: Testing the fixed anvil temperature hypothesis in a
697 cloud-resolving model. *J. Climate*, **20**, 2051–2057.

698 Kushner, P. J., I. M. Held, and T. L. Delworth, 2001: Southern hemisphere atmospheric
699 circulation response to global warming. *J. Climate*, **14 (10)**, 2238–2249.

700 Lacis, A., J. Hansen, P. Lee, T. Mitchell, , and S. Lebedeff, 1981: Greenhouse effect of trace
701 gases, 1970-1980. *Geophys. Res. Lett.*, **8 (10)**, 1035–1038.

702 Lin, B., P. Minnis, and A. Fan, 2003: Cloud liquid water path variations with temperature
703 observed during the Surface Heat Budget of the Arctic Ocean (SHEBA) experiment. *J.*
704 *Geophys. Res.*, **108**, doi:10.1029/2002JD002851.

705 Lin, W. Y. and M. H. Zhang, 2004: Evaluation of clouds and their radiative effects simulated
706 by the NCAR Community Atmospheric Model against satellite observations. *J. Climate*,
707 **17 (17)**, 3302–3318.

708 Lorenz, D. J. and E. T. DeWeaver, 2007: Tropopause height and zonal wind response to

709 global warming in the IPCC scenario integrations. *J. Geophys. Res.*, **112**, D10119, doi:
710 10.1029/2006JD008087.

711 Mace, G. G., E. E. Clothiaux, and T. P. Ackerman, 2001: The composite characteristics
712 of cirrus clouds: Bulk properties revealed by one year of continuous cloud radar data. *J.*
713 *Climate*, **14**, 2185–2203.

714 Manabe, S. and R. T. Wetherald, 1980: On the distribution of climate change resulting from
715 an increase in CO2 content of the atmosphere. *J. Atmos. Sci.*, **37 (1)**, 99–118.

716 Meehl, G. A. e. a., 2007: Global climate projections. *Climate Change 2007: The Physical*
717 *Science Basis*, S. S. et al., Ed., Cambridge University Press, 747–846.

718 Mitchell, J. F. B., C. A. Senior, and W. J. Ingram, 1989: C02 and climate: a missing
719 feedback? *Nature*, **341**, 132–134.

720 Paltridge, G. W., 1980: Cloud-radiation feedback to climate. *Quart. J. Roy. Meteor. Soc.*,
721 **106 (450)**, 895–899.

722 Ramaswamy, V. et al., 2001: Radiative forcing of climate change. *Climate Change 2001:*
723 *The Scientific Basis*, J. T. H. et al., Ed., Cambridge University Press, 350–416.

724 Ringer, M. A., et al., 2006: Global mean cloud feedbacks in idealized climate change exper-
725 iments. *Geophys. Res. Lett.*, **33**, L07718, doi:10.1029/2005GL025370.

726 Roeckner, E., U. Schlese, J. Biercamp, and P. Liewe, 1987: Cloud optical depth feedback
727 and climate modeling. *Nature*, **329**, 138–139.

728 Santer, B. D., et al., 2003: Contributions of anthropogenic and natural forcing to recent
729 tropopause height changes. *Science*, **301 (5632)**, 479–483.

730 Schlesinger, M. E., 1988: Negative or positive cloud optical depth feedback? *Nature*, **335**,
731 303–304.

732 Schneider, S. H., 1972: Cloudiness as a global climatic feedback mechanism: The effects
733 on radiation balance and surface-temperature of variations in cloudiness. *J. Atmos. Sci.*,
734 **29 (8)**, 1413–1422.

735 Schneider, S. H. and R. E. Dickinson, 1974: Climate modeling. *Reviews of Geophysics*,
736 **12 (3)**, 447–493.

737 Schneider, S. H., W. M. Washington, and R. M. Chervin, 1978: Cloudiness as a climatic
738 feedback mechanism: Effects on cloud amounts of prescribed global and regional surface
739 temperature changes in the NCAR GCM. *J. Atmos. Sci.*, **35 (12)**, 2207–2221.

740 Senior, C. and J. Mitchell, 1993: Carbon dioxide and climate. The impact of cloud parame-
741 terization. *J. Climate*, **6**, 393–418.

742 Shindell, D. T., H. Levy, M. D. Schwarzkopf, L. W. Horowitz, J.-F. Lamarque, and G. Falu-
743 vegi, 2008: Multimodel projections of climate change from short-lived emissions due to
744 human activities. *J. Geophys. Res.*, **113**, D11109, doi:10.1029/2007JD009152.

745 Soden, B. J. and I. M. Held, 2006: An assessment of climate feedbacks in coupled ocean-
746 atmosphere models. *J. Climate*, **19**, 3354–3360.

747 Soden, B. J., I. M. Held, R. Colman, K. M. Shell, J. T. Kiehl, and C. A. Shields, 2008:
748 Quantifying climate feedbacks using radiative kernels. *J. Climate*, **21**, 3504–3520.

749 Somerville, R. C. J. and L. A. Remer, 1984: Cloud optical thickness feedbacks in the CO2
750 climate problem. *J. Geophys. Res.*, **89 (D6)**, 9668–9672.

751 Stephens, G. L., 1978: Radiation profiles in extended water clouds. Part II: Parameterization
752 schemes. *J. Atmos. Sci.*, **35 (11)**, 2123–2132.

753 Taylor, K. E. and S. J. Ghan, 1992: An analysis of cloud liquid water feedback and global
754 climate sensitivity in a general circulation model. *J. Climate*, **5 (9)**, 907–919.

755 Tompkins, A. M. and G. C. Craig, 1999: Sensitivity of tropical convection to sea surface
756 temperature in the absence of large-scale flow. *J. Climate*, **12**, 462–476.

757 Trenberth, K. E. and J. T. Fasullo, 2009: Global warming due to increasing absorbed solar
758 radiation. *Geophys. Res. Lett.*, **36**, L07706, doi:10.1029/2009GL037527.

759 Trenberth, K. E. and J. T. Fasullo, 2010: Simulation of present-day and twenty-first-century
760 energy budgets of the southern oceans. *J. Climate*, **23 (2)**, 440–454.

761 Tselioudis, G., A. D. D. Genio, W. Kovari, and M.-S. Yao, 1998: Temperature dependence
762 of low cloud optical thickness in the GISS GCM: Contributing mechanisms and climate
763 implications. *J. Climate*, **11 (12)**, 3268–3281.

764 Tselioudis, G. and W. B. Rossow, 1994: Global, multiyear variations of optical thickness
765 with temperature in low and cirrus clouds. *Geophys. Res. Lett.*, **21(20)**, 2211–2214.

766 Tselioudis, G., W. B. Rossow, and D. Rind, 1992: Global patterns of cloud optical thickness
767 variation with temperature. *J. Climate*, **5**, 1484–1495.

768 Tsushima, Y., et al., 2006: Importance of the mixed-phase cloud distribution in the control
769 climate for assessing the response of clouds to carbon dioxide increase: A multi-model
770 study. *Climate Dyn.*, **27**, 113–126.

771 Vavrus, S., D. Waliser, A. Schweiger, and J. Francis, 2009: Simulations of 20th and 21st
772 century Arctic cloud amount in the global climate models assessed in the IPCC AR4.
773 *Climate Dyn.*, **33**, 1099–1115.

774 Weaver, C. P., 2003: Efficiency of storm tracks an important climate parameter? The
775 role of cloud radiative forcing in poleward heat transport. *J. Geophys. Res.*, **108**, doi:
776 10.1029/2002JD002756.

777 Webb, M., C. Senior, S. Bony, and J. J. Morcrette, 2001: Combining ERBE and ISCCP data
778 to assess clouds in the Hadley Centre, ECMWF and LMD atmospheric climate models.
779 *Climate Dyn.*, **17**, 905–922.

780 Webb, M. J., et al., 2006: On the contribution of local feedback mechanisms to the range of
781 climate sensitivity in two gcm ensembles. *Climate Dyn.*, **27**, 17–38.

782 Wetherald, R. and S. Manabe, 1988: Cloud feedback processes in a general circulation model.
783 *J. Atmos. Sci.*, **45**, 1397–1415.

784 Wetherald, R. T. and S. Manabe, 1980: Cloud cover and climate sensitivity. *J. Atmos. Sci.*,
785 **37 (7)**, 1485–1510.

786 Williams, K. and M. Webb, 2009: A quantitative performance assessment of cloud regimes
787 in climate models. *Climate Dyn.*, **33**, 141–157.

788 Wu, Y., M. Ting, R. Seager, H.-P. Huang, and M. Cane, 2010: Changes in storm tracks and
789 energy transports in a warmer climate simulated by the GFDL CM2.1 model. *Climate*
790 *Dyn.*, 1–20, doi:10.1007/s00382-010-0776-4.

791 Wyant, M. C., C. S. Bretherton, J. T. Bacmeister, J. T. Kiehl, I. M. Held, M. Zhao, S. A.
792 Klein, and B. J. Soden, 2006: A comparison of low-latitude cloud properties and responses
793 in agcms sorted into regimes using mid-tropospheric vertical velocity. *Climate Dyn.*, **27**,
794 261–279.

795 Yin, J. H., 2005: A consistent poleward shift of the storm tracks in simulations of 21st
796 century climate. *Geophys. Res. Lett.*, **32**, L18701, doi:10.1029/2005GL023684.

797 Zelinka, M. D. and D. L. Hartmann, 2010: Why is longwave cloud feedback positive? *J.*
798 *Geophys. Res.*, **115**, D16117, doi:10.1029/2010JD013817.

799 Zhang, M. H. e. a., 2005: Comparing clouds and their seasonal variations in 10 atmospheric
800 general circulation models with satellite measurements. *J. Geophys. Res.*, **110**, D15S02,
801 doi:10.1029/2004JD005021.

List of Figures

7 As in Figure 6, but for the 50°-70°S region.

8 Zonal mean ensemble mean (a) LW, (b) SW, and (c) net cloud feedbacks partitioned into components due to the proportionate change in cloud fraction, change in cloud vertical distribution, change in cloud optical depth distribution, and residual term. The abscissa is sine of latitude so that the visual integral is proportional to Watts per Kelvin of mean surface temperature change. The ensemble mean refers to all models except the *uiuc* and *mpi_echam5* models.

9 Global mean cloud feedbacks estimated for each model using (green) the adjusted change in cloud radiative forcing technique of Soden et al. (2008) and (black) cloud radiative kernels. Also shown is the contribution to the feedback of (blue) amount, (cyan) altitude, (red) optical depth, and (maroon) residual changes.

10 Global mean (red) LW, (blue) SW, and (black) net cloud feedback estimates and the contribution to the cloud feedbacks from the proportionate change in cloud fraction, change in cloud vertical distribution, change in cloud optical depth distribution, and residual term. Each model is represented by a dot and the multi-model mean is represented by the height of the vertical bar. The *uiuc* and *mpi_echam5* models are excluded from this figure.

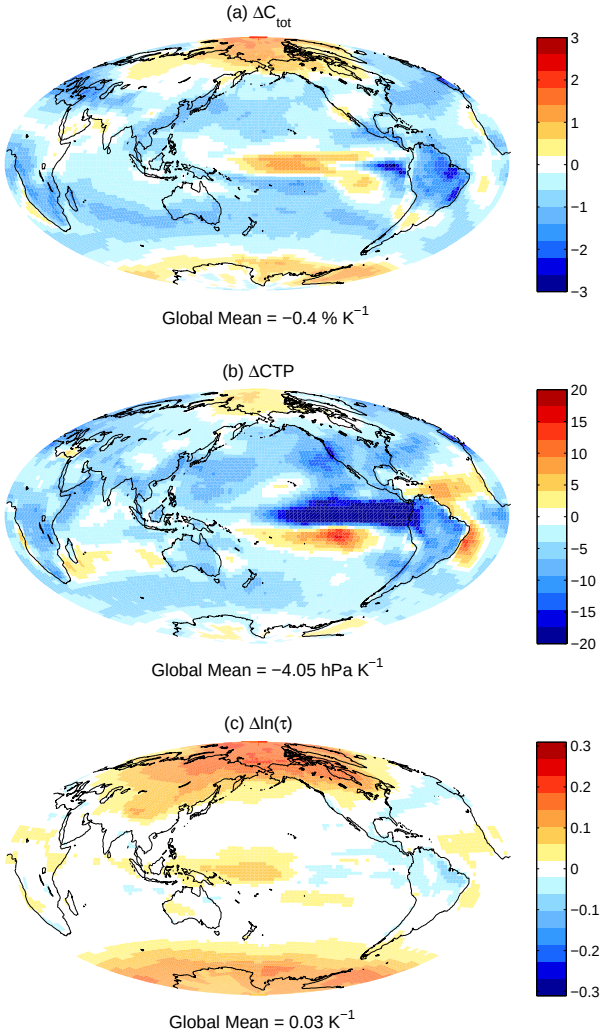

FIG. 1. Ensemble mean change in (a) cloud fraction, (b) cloud fraction-weighted pressure, and (c) cloud fraction-weighted natural logarithm of optical depth. The ensemble mean refers to all models except the *uiuc* and *mpi_echam5* models, which are excluded based on discrepancies discussed in the companion paper.

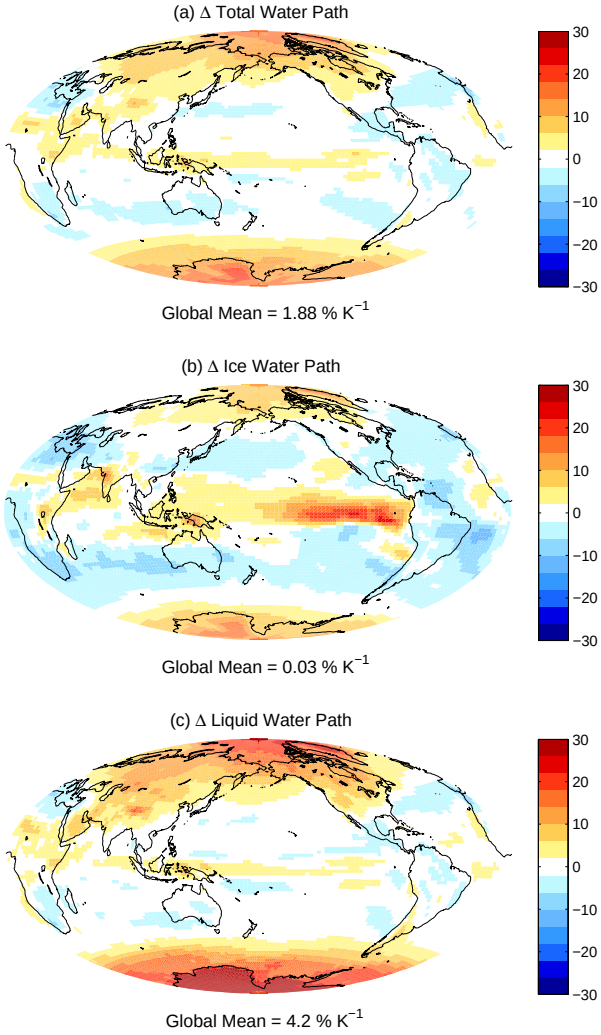

FIG. 2. Ensemble mean change in (a) total water path, (b) ice water path, and (c) liquid water path. The ensemble mean refers to all models except the *uiuc* and *mpi_echam5* models. The *bmrc1*, *ipsl_cm4*, and *miroc_hisens* models are also excluded because they did not archive total water path or ice water path.

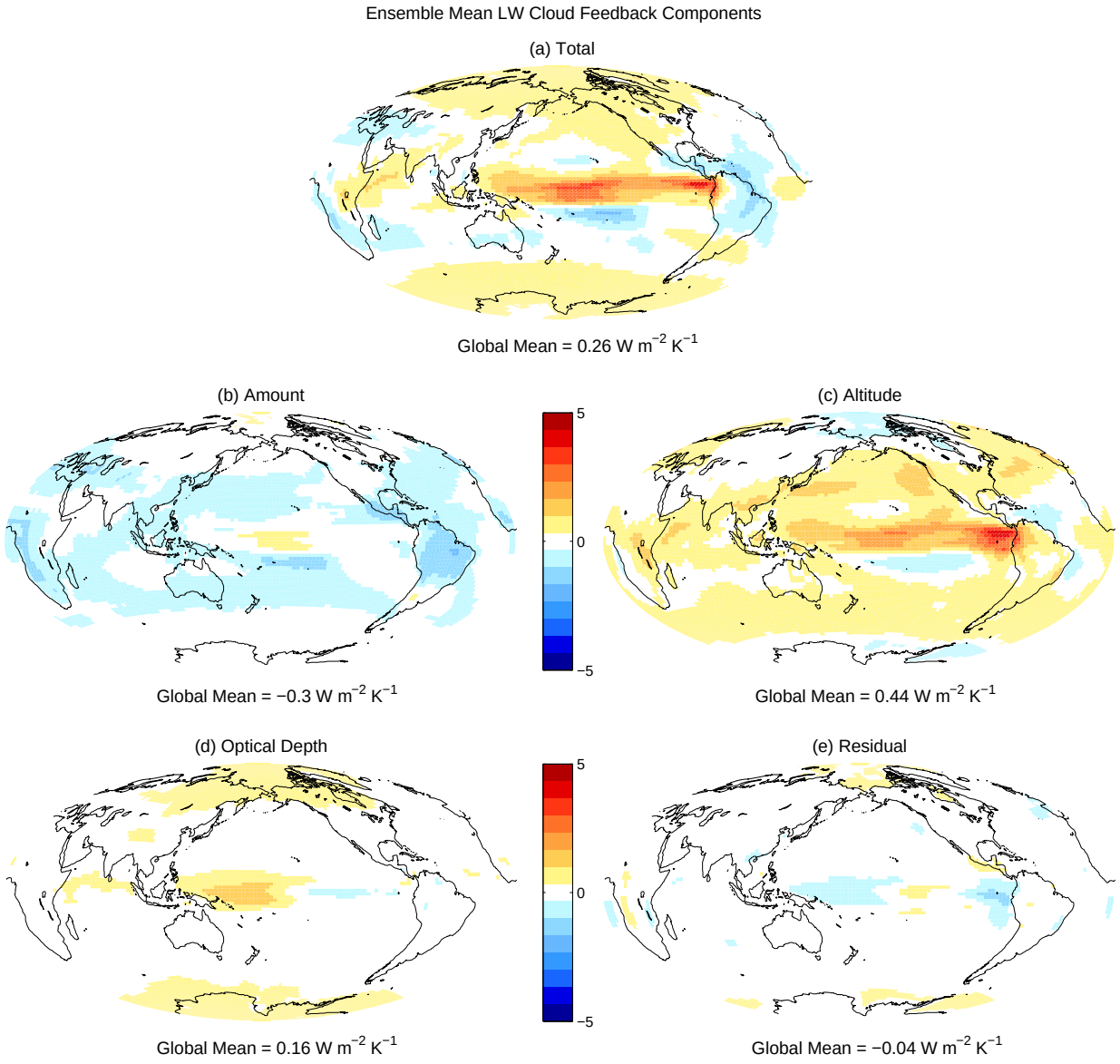

FIG. 3. Ensemble and annual mean (a) LW cloud feedback and components due to the (b) proportionate change in cloud fraction, (c) change in cloud vertical distribution, (d) change in cloud optical depth distribution, and (e) residual term. The ensemble mean refers to all models except the *uiuc* and *mpi_echam5* models.

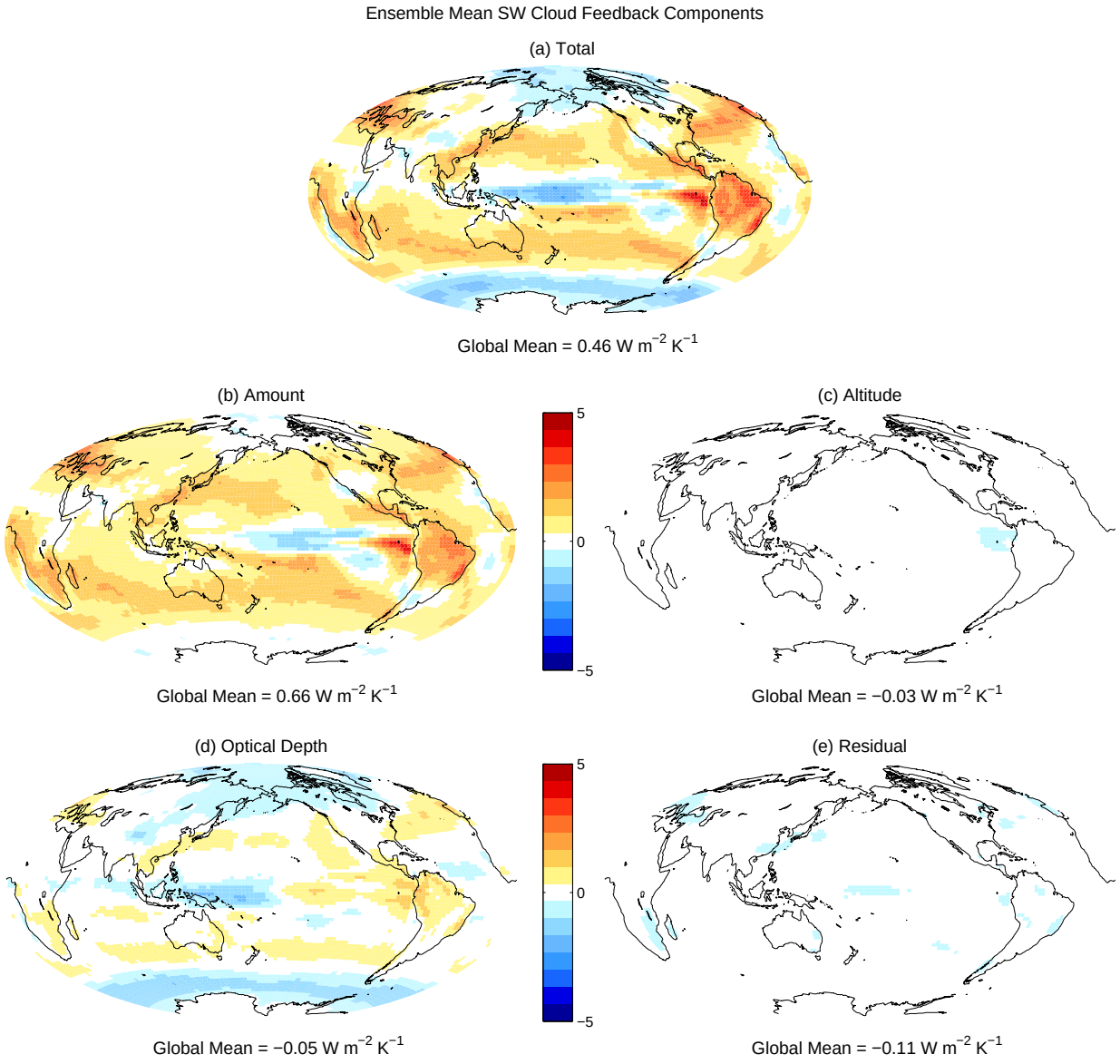

FIG. 4. As in Figure 3, but for the SW cloud feedback partitioning.

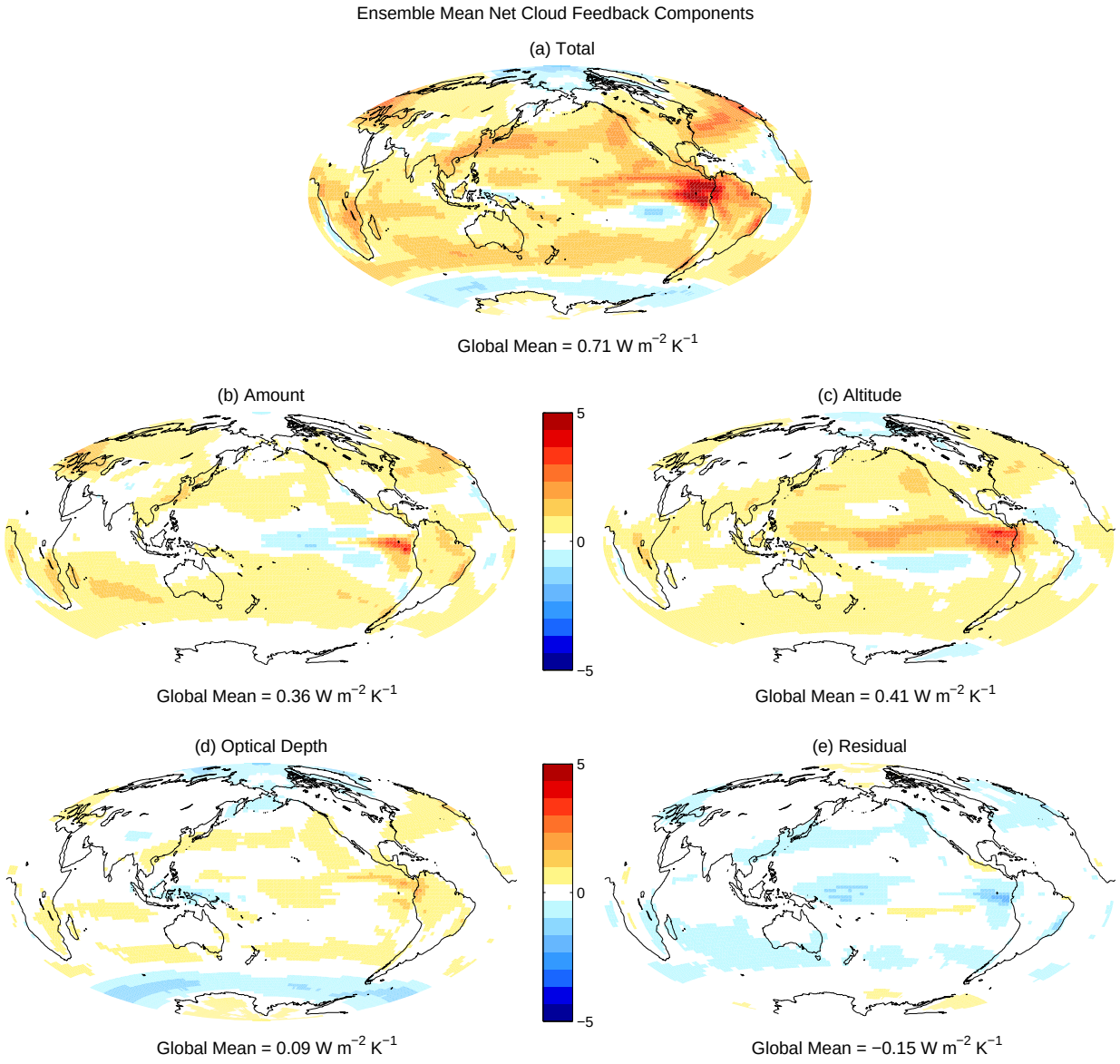

FIG. 5. As in Figure 3, but for the net cloud feedback partitioning.

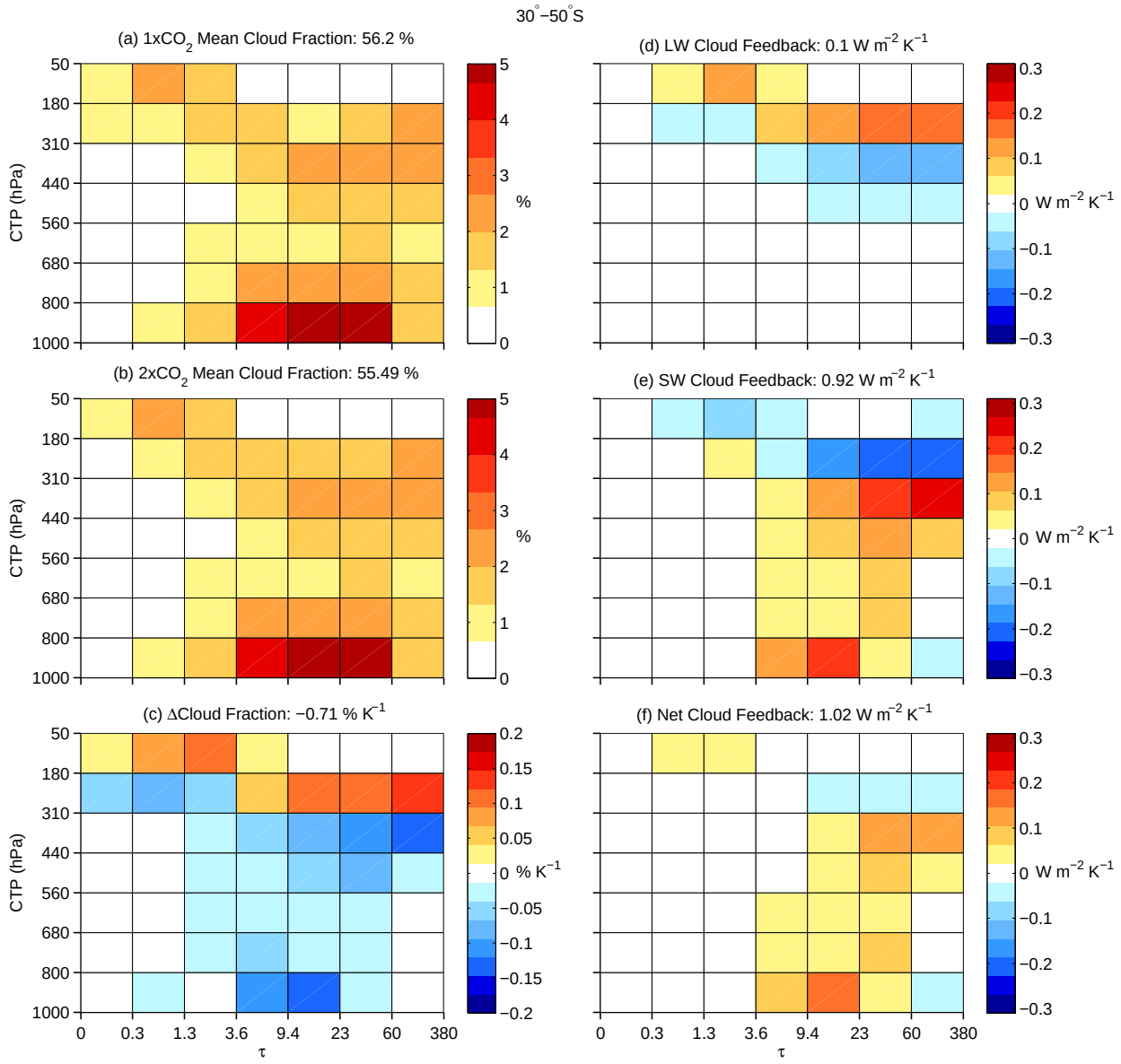

FIG. 6. Mean cloud fraction in the 30°-50°S region for the (a) 1xCO$_2$ and (b) 2xCO$_2$ runs of all models except *uiuc* and *mpi_echam5*, along with (c) the difference expressed per unit change in each model's global mean surface temperature between the two states. Multiplication of the histogram of the change in cloud fraction with the (d) LW, (e) SW, and (f) net cloud radiative kernel histogram. The sum of each histogram is shown in each title.

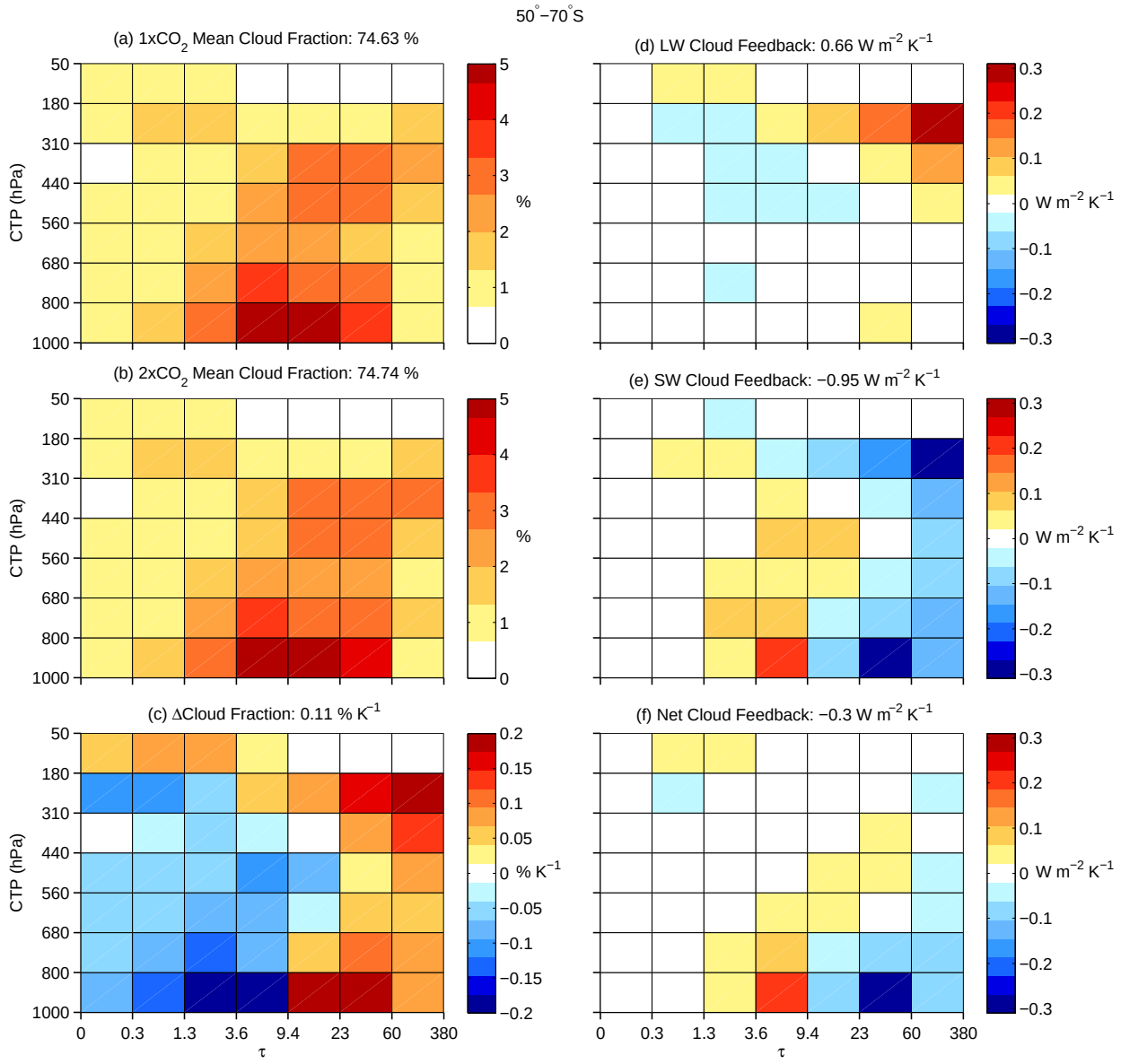

FIG. 7. As in Figure 6, but for the 50°-70°S region.

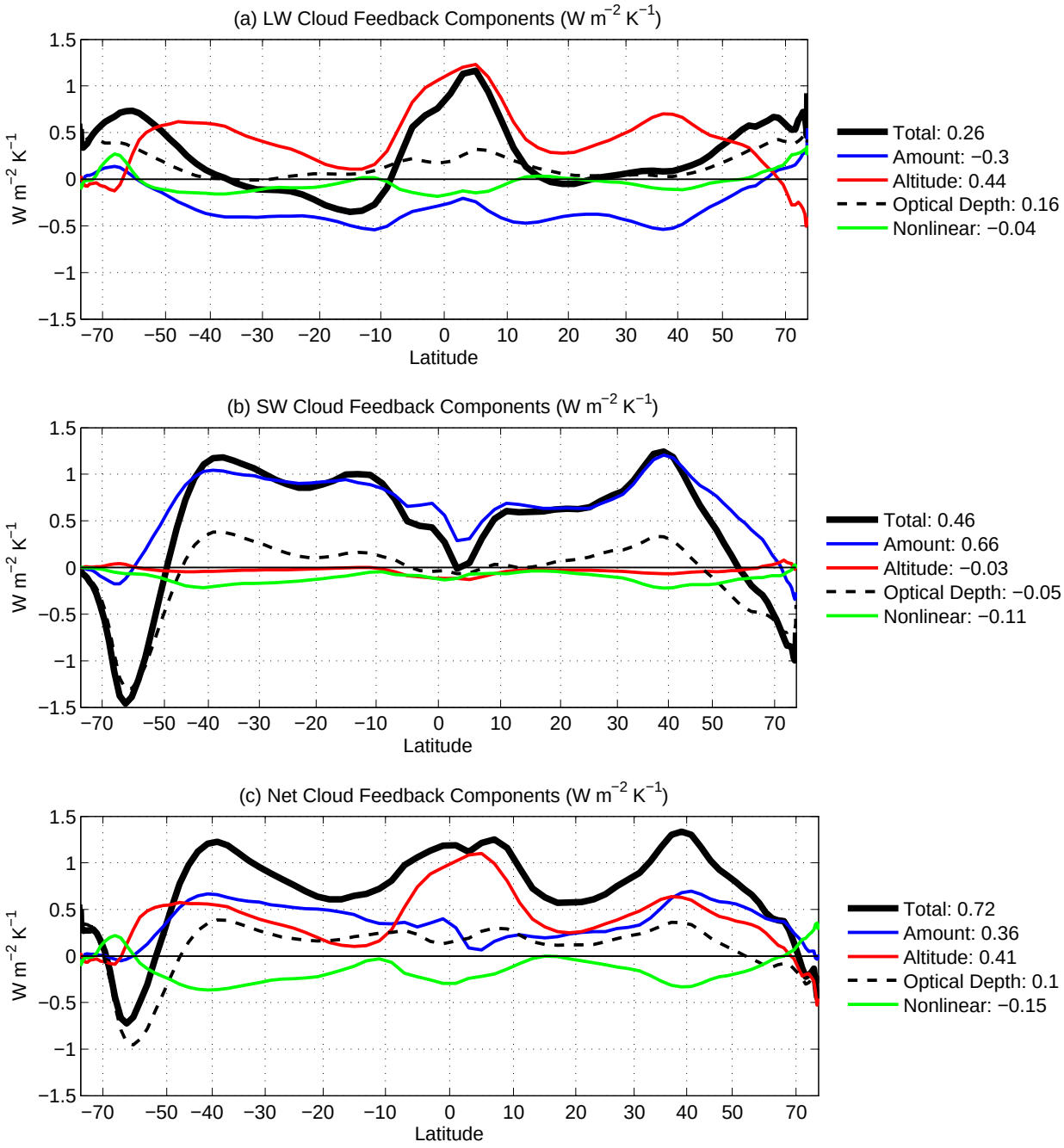

FIG. 8. Zonal mean ensemble mean (a) LW, (b) SW, and (c) net cloud feedbacks partitioned into components due to the proportionate change in cloud fraction, change in cloud vertical distribution, change in cloud optical depth distribution, and residual term. The abscissa is sine of latitude so that the visual integral is proportional to Watts per Kelvin of mean surface temperature change. The ensemble mean refers to all models except the *uiuc* and *mpi_echam5* models.

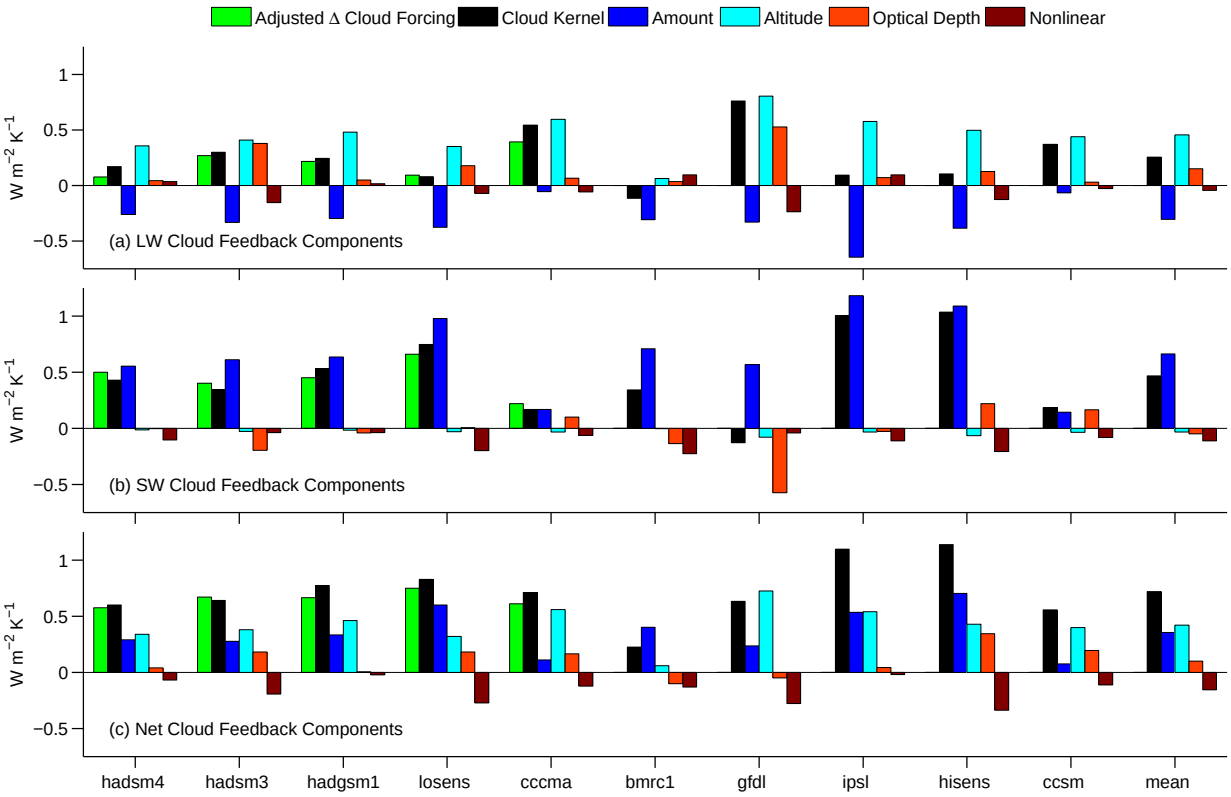

FIG. 9. Global mean cloud feedbacks estimated for each model using (green) the adjusted change in cloud radiative forcing technique of Soden et al. (2008) and (black) cloud radiative kernels. Also shown is the contribution to the feedback of (blue) amount, (cyan) altitude, (red) optical depth, and (maroon) residual changes.

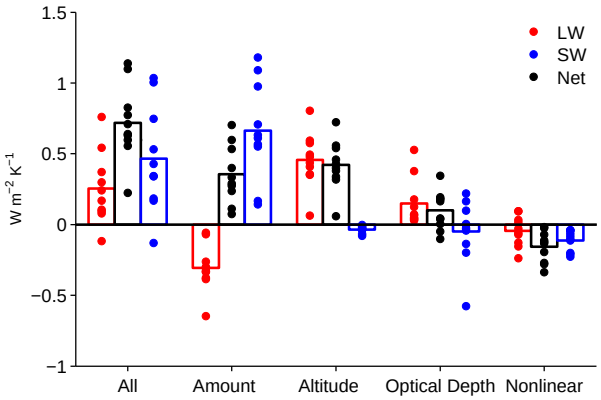

FIG. 10. Global mean (red) LW, (blue) SW, and (black) net cloud feedback estimates and the contribution to the cloud feedbacks from the proportionate change in cloud fraction, change in cloud vertical distribution, change in cloud optical depth distribution, and residual term. Each model is represented by a dot and the multi-model mean is represented by the height of the vertical bar. The *uiuc* and *mpi_echam5* models are excluded from this figure.